Water Air Soil Pollut (2022) 233:442
https://doi.org/10.1007/s11270-022-05912-2

Relative Empirical Evaluation of the Aqueous Sequestration of Methylene Blue Using Benzene-1,4-dicarboxylic Acid-Linked Lanthanum and Zinc Metal Organic Frameworks

Emmanuel B. AttahDaniel · Fanyana M. Mtunzi · Donbebe Wankasi · Nimibofa Ayawei · Ezekiel D. Dikio · Paul N. Diagboya

Received: 19 September 2022 / Accepted: 17 October 2022

Abstract Two metal–organic frameworks (MOFs), lanthanum-1,4-benzene dicarboxylate (LaBDC) and zinc-1,4-benzene dicarboxylate (ZnBDC) were synthesized via the reflux-controlled solvothermal process. The characterization of both adsorbents confirmed the physicochemical properties of well-defined surface morphology with high porosity and thermal stability greater than 450 °C. Adsorption of methylene blue (MB) using both MOFs showed that the rate of MB removal reached equilibrium at 120 and 30 min for LaBDC and ZnBDC, respectively. The MB adsorption was pH dependent with optimum adsorption at pH 12, and the adsorption data trend fitted the fractal pseudo-second-order model (FPSOM), Langmuir and Freundlich adsorption isotherm models, and MB adsorption capacities of LaBDC and ZnBDC are 35.0 and 55.0 mg/g, respectively. The process is physisorption, spontaneous, and feasible. The ZnBDC MOF had a better potential for the removal of MB from an aqueous solution than LaBDC. Both MOFs have the potential to sequester MB from aqueous phases but can be enhanced for better performance.

Keywords Metal–organic framework · Lanthanum · Zinc · Adsorption · Methylene blue

1 Introduction

Water contamination has become a global concern due to population growth and industrialization, which exert enormous pressure on the quantity and quality of potable water supply. According to reports, between 5 and 10 million people are poisoned yearly from the consumption of contaminated water (Savin & Butnaru, 2008). Prominent environmental water contaminants range from toxic metals (such as Pb(II), Cd(II), As(III), Cr(VI), and Hg(II)I) to organic contaminants (such as pesticides, polycyclic aromatic hydrocarbons, and dyes) (Diagboya et al., 2021a, 2021b; Olu-Owolabi et al., 2022; Sera et al., 2022; Zanele et al., 2021). The persistence and continuous increase of these contaminants in water and their concomitant health effects have resulted in enhanced

PN Diagboya is a visiting scientist at Institute for Soil Science and Soil Conservation, Justus Liebig University, Gießen, Germany.

E. B. AttahDaniel · F. M. Mtunzi · P. N. Diagboya (✉)
Environmental Fate of Chemicals and Remediation Laboratory, Department of Biotechnology and Chemistry, Vaal University of Technology, VanderbijlparkGauteng 1911, South Africa
e-mail: pauldn2@yahoo.com

D. Wankasi · E. D. Dikio
Department of Chemical Sciences, Faculty of Sciences, Niger Delta University, Wilberforce Island, Amassoma, Nigeria

N. Ayawei
Department of Chemistry, Bayelsa Medical University, Bayelsa State, Yenagoa, Nigeria

Published online: 29 October 2022

efforts to develop new or more effective remediation strategies for processing potable water.

One major class of organic contaminants in the water is a dye. Dyes are found in wastewater released from textile, cosmetics, leather, paper, food, and several other industries as effluents into freshwater bodies (Diagboya et al., 2014; Liu et al., 2016). An estimated 2.8×10^5 tons of dyes are discharged into water bodies from more than 7×10^5 tons of 10,000 different types of dyes that are produced annually worldwide (Lin, 2015; Mohammed & Jaarrod, 2010; Zhang et al., 2017). These effluents that are usually discharged without adequate treatment exert adverse effects, such as reducing water quality and lowering aquatic photosynthetic activities due to decreased light penetration for the sustenance of aquatic plants. Methylene blue (MB), a cationic dye is of utmost concern in water treatment studies because it contains a similar cationic moiety as found in most reactive dyes employed in the pulp and paper, printing, textile, and leather industries. It is difficult to degrade because it contains benzene rings and N and S atoms, which also make it toxic, mutagenic, teratogenic, and cause serotonin syndrome (a red blood cells breakdown caused by the conversion of ferric iron in hemoglobin to ferrous iron), and irritation of the skin and the eyes. Other health effects include high blood pressure, shortness of breath, confusion, headache, profuse sweating, and vomiting (Ayati et al., 2016; Diagboya & Dikio, 2018b; Liu et al., 2016; Okoli et al., 2017; Zhao et al., 2015). Consequently, the need to ameliorate these challenges to human health and the environment cannot be overemphasized. Methods such as oxidation, biodegradation, photo-degradation, and adsorption (Mohammed & Jaarrod, 2010) are used for dye removal from wastewater, and adsorption is the most popular of these. Dyes are well known for their stability in the presence of light and heat, and resistance to oxidation and biodegradation, but are easily removed via adsorption (Ayati et al., 2016; Fallah Shojaei et al., 2018). Hence, adsorption has become the main strategy of focus for researchers in dye wastewater remediation studies. Thus, different types of adsorbent materials (natural and synthetic) have been reported for the removal of dyes from wastewater. Biosorbents prepared from agricultural wastes provide low-cost and environmentally friendly adsorbents for dye removal from wastewater. They can be used in their original or modified forms as pristine biomass and activated charcoal. These include maize cob (Juang et al., 2002), rice hulls, fruit peels, stones and nutshells (Aygün et al., 2003; Hameed & Hakimi, 2008), bagasse/sugar beet pulp (Malekbala et al., 2012; Valix et al., 2004), coir pith (Namasivayam & Kavitha, 2002), banana pith (Kadirvelu et al., 2000), straw, rice husk (Malik, 2003; Mohamed, 2004), and pinewood, sawdust (Malik, 2003) and bamboo (Guo et al., 2014). Other adsorbents include red mud (Wang et al., 2019), sludge (Jahagirdar et al., 2015), magnetic graphene oxide (Farooq Khan et al., 2022b), magnetic gum acacia hydrogel (Farooq Khan et al., 2022a), metal hydroxides (Starukh, 2017), and fly ash (Ge et al., 2018). These adsorbents have disadvantages (low adsorption capacity, high cost of activated carbon due to large energy requirement, non-selectivity and secondary waste generation, and problem of regeneration) which have compelled renewed research for alternative adsorbents with high adsorption efficiencies to effectively remove dyes from wastewater (Lin, 2015; Zhang et al., 2016; Zhao et al., 2015). New adsorbents like metal–organic frameworks and hybrid composites possess merits such as high specific surface area, large pore volumes, ability to tailor their pore sizes and regulate adsorption capacity (Akpotu et al., 2022b; Ali, 2012; DeCoste & Peterson, 2014; Gangadhar et al., 2012; Hasan & Jhung, 2015; Hasan et al., 2013) have been reported to exhibit potentially improved properties for the removal of the toxic benzene ring and N and S atoms containing contaminants from aqueous media (Fallah Shojaei et al., 2018; Gong et al., 2018; Nakhla, 2009; Namasivayam and Kavitha; Sriram et al., 2021; Wang et al., 2017).

Metal–organic frameworks (MOFs) are a class of porous materials that consist of bridging ligand (organic linker) bonded via coordination bonds to a transition metal ion (secondary building unit (SBU)) (Bosch et al., 2017; Dikio & Farah, 2013; Nakhla, 2009; Sriram et al., 2021). They have found application in areas such as catalysis (Mulfort et al., 2009), hydrogen storage (Schoedel et al., 2016), methane storage (Lin et al., 2016), and drug delivery (Horcajada et al., 2006; Munoz et al., 2003). A previous study in our laboratory reported that cadmium-organic framework (Cd-H_4bta) exhibited good potential for the removal of Cu(II), Pb(II), and Ni(II) with adsorption capacities of 183.4, 171.4, and 120.3 mg/g, respectively (Shooto & Dikio,

2018). Similarly, Cu-MOF (Cu-BTC) expressed excellent capacity for the adsorption of MB from wastewater (Lin et al., 2014), while a composite $H_6P_2W_{18}O_{62}$ (MOF-5) demonstrated significantly enhanced MB adsorption efficiency of approximately 195 mg/g from aqueous medium (Mulugeta & Lelisa, 2014). Therefore, since only a few studies have reported adsorption of MB on MOFs, the objective of this study was to synthesize 1,4 benzene dicarboxylic linked lanthanum (lanthanum-1,4-benzene dicarboxylate (LaBDC)) and zinc metal–organic frameworks (zinc-1,4-benzene dicarboxylate (ZnBDC)) via the solvothermal reflux-controlled method for the removal of MB from aqueous media.

2 Materials and Method

2.1 Materials and Preparation of Metal–Organic Frameworks (MOFs)

Ultra-pure water and analytical-grade chemicals were used throughout this study. The chemicals include terephthalic acid ($C_8H_6O_6$) (> 99%) (Acros Organics), N,N-dimethylformamide (DMF) (Promark Chemicals), methanol (CH_3OH) (99.99%) (Promark chemicals), lanthanum (III) nitrate, hexahydrate, ($LaN_3O_9.6H_2O$) (Merck) zinc nitrate hexahydrate ($Zn(NO_3)_2.6H_2O$ (Merck), and methylene blue (MB) (Labochem).

Lanthanum-organic framework (LaBDC) and Zinc-organic framework (ZnBDC) were prepared according to the reported method (Shooto et al., 2016). The LaBDC was prepared by dissolving $La(NO_3)_3.6H_2O$ (0.02008 mol) and terephthalic acid (0.02008 mol) in 80 mL of dimethylformamide (DMF) in a 250-mL round bottom flask. This was refluxed under mild stirring for 12 h at 105 °C. The reaction products were centrifuged, collected, and washed with methanol thrice, dried at 75 °C for ≈ 6 h, and preserved for further use. Similarly, the ZnBDC was prepared by dissolving $Zn(NO_3)_2.6H_2O$ (0.02008 mol) and terephthalic acid (0.02008 mol) in 80 mL of DMF in a 250-mL round bottom flask. This was refluxed under mild stirring for 8 h at 105 °C. Treatment of the product was as stated above.

2.2 Characterization of LaBDC and ZnBDC Adsorbents

The adsorbents were characterized using a scanning electron microscope (SEM), (Zeiss Auriga Field Emission, Germany), energy dispersive X-ray (EDX) (attached to an Oxford *X*-max detector equipped with Aztec software), the Brunauer–Emmett–Teller (BET) surface area was determined by a Micrometrics TriStar 113,020 (USA), Fourier transform infrared (FTIR) spectrophotometer (Thermo Scientific, NICOLET iS50, USA), powder X-ray diffraction (pXRD) (Shimadzu XRD-7000, USA), thermogravimetric analyzer (TGA) (Perkin Elmer TGA 4000, PerkinElmer Instruments, Waltham, MA). The pH at the point of zero charges (pHpzc) of both MOFs was determined using the solid addition method (Zanele et al., 2021).

2.3 Batch Adsorption Studies Using the LaBDC and ZnBDC Adsorbents

A stock solution of 1000 mg/L of MB was prepared for use throughout the study. The working solutions were prepared from this stock solution via serial dilution. Replicates batch adsorption studies of MB blue using 20 mg of either LaBDC or ZnBDC were carried out in 20 mL of 50 mg/L MB in 50-mL plastic vials. The mixtures of MB/MOFs were equilibrated at 200 rpm on an electric shaker. For the effect of time or rate of MB adsorption, similar tubes representing varying times from 1 to 240 min were equilibrated; tubes representing a particular time were withdrawn from the shaker at the appropriate time, centrifuged at 4000 rpm for 10 min, and the supernatant used to determine the amount of MB left in the solution. It was observed that adsorption equilibrium was established within 120 min for LaBDC and 30 min for ZnBDC. Subsequent parameters such as effects of pH (2–12), initial MB concentration (20–60 mg/L), and ambient temperature (300, 310, and 320 K) were studied adopting the equilibrium time of 120 and 30 min for LaBDC and ZnBDC, respectively, using 20 mL of MB solution and 20 mg of each adsorbent.

2.4 Data Treatment

The initial concentration (C_o) and final concentration (C_e) of MB concentration in solution were used to

calculate the amount of MB adsorbed q_e (mg/g) using Eq. 1.

$$q_e = (C_O - C_e)v/m \tag{1}$$

where v and m are the volume of the solution (mL) and mass (g) of adsorbent used, respectively.

The nonlinear pseudo-first-order (PFO) model (Eq. 2) and pseudo-second-order (PSO) model (Eq. 3) (Lagergren, 1898), the Webber–Morris intraparticle diffusion (IPD) kinetics model (Eq. 5) (Weber and Morris, 1963), and the homogenous fractal pseudo-second-order model (FPSOM) (Eq. 4) (Haerifar & Azizian, 2014; Olu-Owolabi et al., 2021) were used in modeling the data.

$$q_t = q_e(1 - e^{-k_1 t}) \tag{2}$$

$$q_t = \frac{q_e^2 k_2 t}{1 + q_e k_2 t} \tag{3}$$

$$q_t = \frac{k_f q_e^2 t^{\alpha}}{1 + k_f q_e t^{\alpha}} \tag{4}$$

$$q_e = k_{IPD} t^{1/2} + C \tag{5}$$

where q_e and q_t are the quantity of MB adsorbed (mg/g) at equilibrium and time t, respectively; k^1 (/min) and k^2 (g/mg/min) are the rate constants of the PFO and PSO, respectively. The k_i (g/g/min$^{1/2}$) is the rate parameter of IPD control stage and C is the surface concentration of MB on LaBDC and ZnBDC. The model parameters obtained were computed using Origin 8 software.

The equilibrium adsorption data were analyzed using the Langmuir (Langmuir, 1916) (Eq. 6) and Freundlich adsorption isotherm models (Freundlich, 1907) (Eq. 7).

The Langmuir adsorption isotherm model is given as

$$q_e = \frac{Q_O b C_e}{1 + bC_e} \tag{6}$$

The Freundlich adsorption isotherm is given by Eq. (7).

$$q_e = k_f C_e^n \tag{7}$$

where Q_o is the maximum adsorption capacity per unit weight of adsorbent, b is a solute–surface interaction energy-related parameter, q_e and C_e are same as above, and k_f is the Freundlich isotherm constant. and n is the model linearity parameter.

The thermodynamic parameters—enthalpy change (ΔH^o) and entropy change (ΔS^o)—were obtained using the equilibrium adsorption data at 300, 310, and 320 K by first determining the value of K_c using Eq. 8 for all data points

$$K_C = \frac{q_e}{C_e} \tag{8}$$

The K_c values of each point were plotted against q_e values to obtain the values of Kc for each temperature. The ln Kc values were then plotted against the reciprocal of the temperatures to obtain the parameters in Eq. 9. The Gibbs free energy of sorption ΔG^o, which is a fundamental criterion for spontaneity, was obtained from Eq. 9.

$$\Delta G^o = -\mathrm{RTL}nK_C \tag{9}$$

$$LnK_C = \frac{\Delta S^o}{R} - \frac{\Delta H^o}{RT} \tag{10}$$

3 Results and Discussion

3.1 Physicochemical Properties

The FTIR spectra analysis (Fig. 1a) of the linker exhibited a $-$OH broad peak at 3200 cm^{-1}. This –OH group in the linker was transferred to both MOFs, which exhibited weaker $-$OH broads that were comparatively stronger in the ZnBDC, where it was expressed at 3158 cm^{-1}. The –C=O peak vibrations in both the linker and MOFs were observed at 1572, 1508, and 1421 cm^{-1}, respectively, while the peak for the $-$C$-$H bending vibration in all three spectra was observed at 1277 cm^{-1}. The $-$C$-$N stretching vibrations were observed in LaBDC at 1107.1 cm^{-1} and at 1110.4 cm^{-1} for ZnBDC; since the synthesis did not intentionally involve nitrogen, it has been reported that the DMF used for the synthesis process is the source of this nitrogen in both MOFs (Prabhu et al., 2019; Zhu et al., 2012). Sharp peaks attributed to benzene ring $-$C$-$H bending vibrations were observed

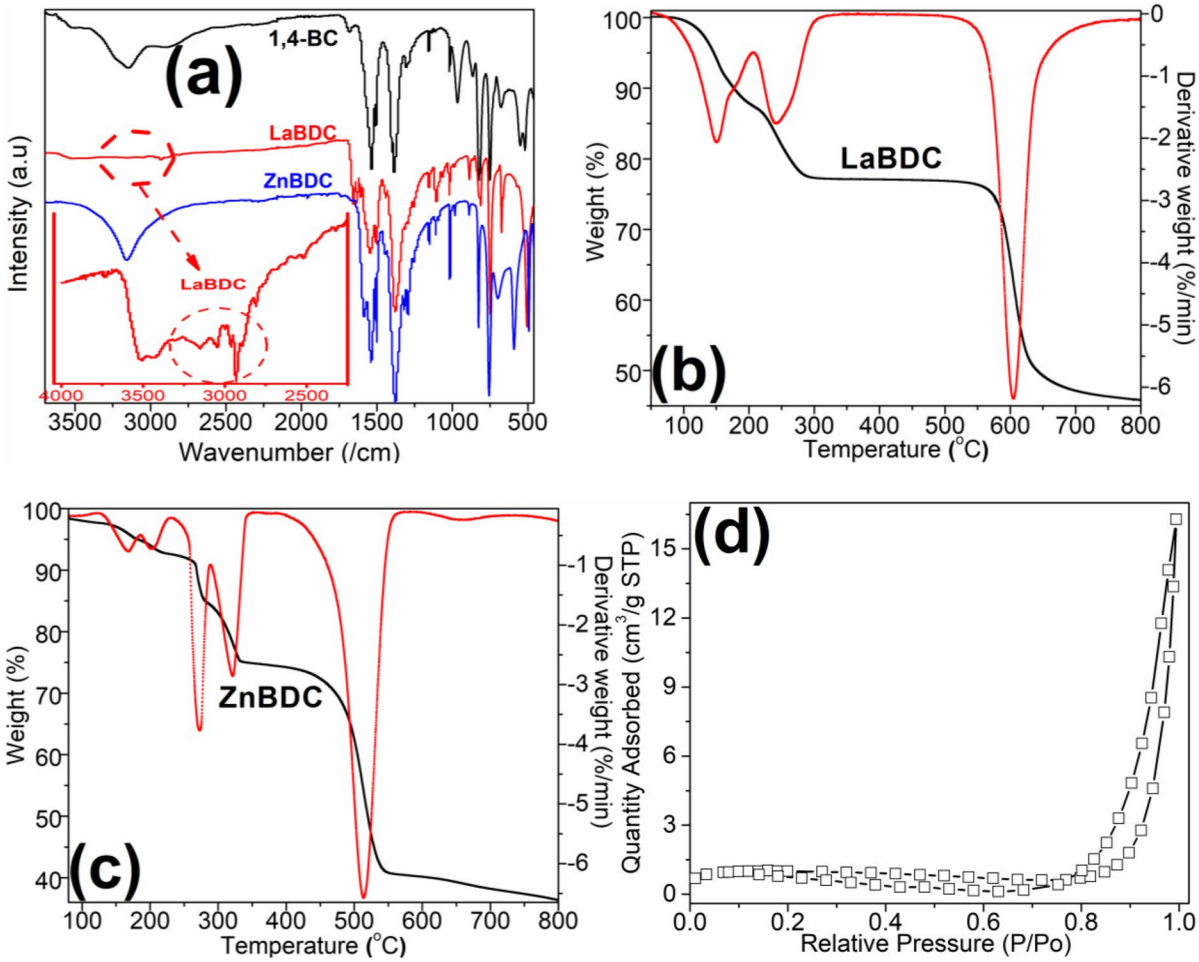

Fig. 1 (**a**) Comparison of FTIR spectra of 1,4-BDC, LaBDC and ZnBDC (insert: LaBDC spectra region between 2250 and 4044 cm^{-1}); TGA and DTA spectra of **b** LaBDC and **c** ZnBDC; **d** typical N_2 adsorption–desorption BET isotherm depicted for the ZnBDC at 77 K

at 747 cm^{-1} (LaBDC) and at 825.7 cm^{-1} (ZnBDC). Metal–oxygen bond bending and stretching vibrations due to the La–O bond in LaBDC were identified at 504.5 and 444.4 cm^{-1}, respectively (Chen et al., 2016; Hosseini et al., 2020; Prabhu et al., 2019), while the sharp peak at 492.3 cm^{-1} was ascribed to Zn − O stretching vibration in ZnBDC (Hosseini et al., 2016; Wang et al., 2014; Wlodarski et al., 2020).

The thermal stabilities of the synthesized MOFs are presented in Fig. 1b, c. The thermogram for LaBDC (Fig. 1b) and ZnBDC (Fig. 1c) show three stages of weight loss by both MOFs with or as the temperature increased. The first degradation step (≈ 14% weight loss) of LaBDC occurred between 100 and 225 ℃ while in ZnBDC, it occurred at between 30 and 240 ℃ (≈ 10% weight loss), and this could be attributed to the expulsion of water of crystallization, trapped DMF molecules and trace of methanol (deployed in washing the MOFs after preparation). Between 225 and 290 ℃, the second degradation stage (≈ 9% weight loss) for LaBDC was observed, and for ZnBDC, it was around 240 and 370 ℃ (≈ 19% weight loss). This later stage was ascribed to the decomposition of carbonates in the two materials (Prabhu et al., 2019). The third stage of degradation leading to the collapse of the coordination bonds and dissociation of the ligands (La and Zn) ions in the LaBDC and ZnBDC frameworks were observed between 581 and 633 ℃ (≈ 27% weight loss) for LaBDC; between 450 and 525 ℃ (≈ 30% weight

loss) for ZnBDC. The three stages of degradation were clearly depicted by the differential thermogram (DTA) (red lines in Fig. 1b and c), showing the three areas of endothermic heat of absorptions that tally with the weight losses in the three stages.

The porosities of both MOFs were studied using the BET analysis. The nitrogen adsorption–desorption isotherms at 77 K for the LaBDC adsorbent (not shown) revealed a type II isotherm (hysteresis within the range of $P/P_o = 0.0$ to 0.9) with the vertical tail observed at $P/P_{o\ =}$ 0.9, indicating that LaBDC is a microporous material (Aghajanloo et al., 2014; Liu et al., 2008). A similar isotherm was also observed for the ZnBDC (Fig. 1d), which also indicates that it is a microporous material. The region of the curve between $P/P_o = 0.1$–0.8, which is almost linear, revealed the end of monolayer adsorption, while the knee between $P/P_o = 0.0$–0.1 indicated the commencement of multilayer adsorption in the adsorbent ZnBDC. The pore size and volume of the LaBDC MOF are 17.90 nm and 0.0022 cm^3/g, while those for the ZnBDC MOF are 24.35 nm and 0.0207 cm^3/g, respectively.

The XRD diffraction patterns of both MOFs are depicted in Fig. 2a and b. These diffraction patterns correspond to the diffraction patterns obtained for similar MOFs prepared via the hydrothermal method (Chen et al., 2017) as well as that prepared using the solvothermal method (Prabhu et al., 2019) with a sharp peak at 2θ of 8.60°, indexed at 220, and a cubic crystal structure (Fm = 3 m) (Liu et al., 2009). A sharp crystalline peak at 2θ of 21.82° was recorded for ZnBDC (Fig. 2b). The X-ray diffraction reference code JCPDS no. 00–055-1863 confirms the peak positions and intensities of the ZnBDC (Li et al., 1998).

The EDX elemental analysis of LaBDC (Fig. 2a insert) and ZnBDC (Fig. 2a insert) showed that the LaBDC consists of C, La, and O at 47.7,

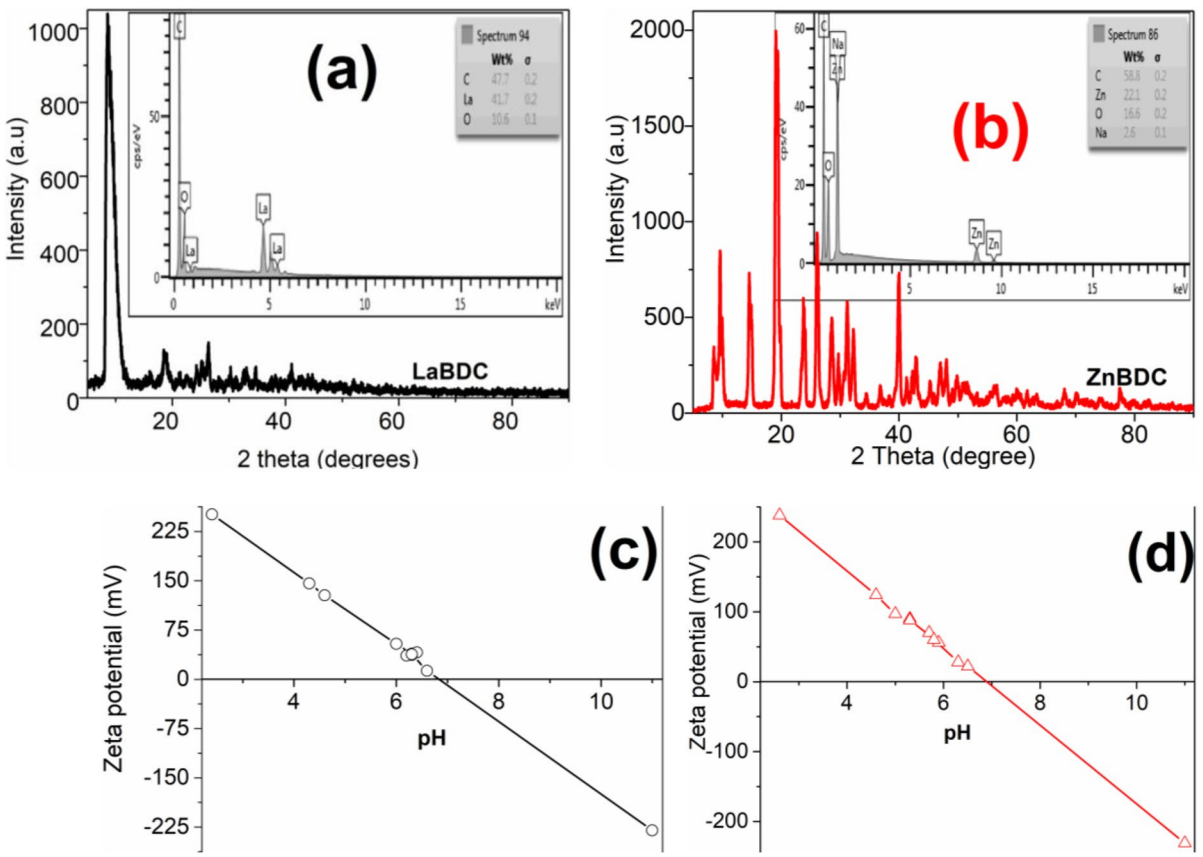

Fig. 2 X-ray diffractograms of **a** LaBDC (insert: LaBDC EDX result) and **b** ZnBDC (insert: ZnBDC EDX result); plots of zeta potential versus pH showing the pH at point of zero charge (pHpzc) for **c** LaBDC and **d** ZnBDC

41.7, and 10.6%, respectively, while ZnBDC contained C, Zn, and O at 58.8, 22.1, and 16.6%, respectively, with 2.6% Na present as impurity; this could have been introduced by the precursors used for the synthesis.

The performance of an adsorbent is a function of the degree of the charge density around it and in the adsorbate (Altenor et al., 2009; Diagboya et al., 2019; Zanele et al., 2021). Hence, we evaluated the pH at the point of zero charges (pHpzc) of both MOFs, which was observed within the pH range of 2–12 (Fig. 2c and d). The pHpzc of both MOFs were the same and at 6.8; this indicates that the surfaces of these materials would be electron-accepting (positively charged) between pH 2 and 6.7, while they would be electron donating (negatively charged) at a pH range of 6.9 and 12.

The SEM micrographs of the synthesized LaBDC and ZnBDC are presented in Fig. 3a–d. The morphological features of LaBDC showed well-defined cubic shapes and irregular surfaces (Fig. 3a and b). The ZnBDC at 100 nm magnification (Fig. 3c) showed interwoven structures that became irregular shapes when observed at 200 nm (Fig. 3d).

3.2 Adsorption Studies

3.2.1 Effect of Time on MB Adsorption on the MOFs and the Adsorption Kinetics

The adsorption performances of LaBDC and ZnBDC were evaluated using MB. The rate of MB uptake by the two MOFs and the establishment of equilibrium adsorption time was accessed by the varying

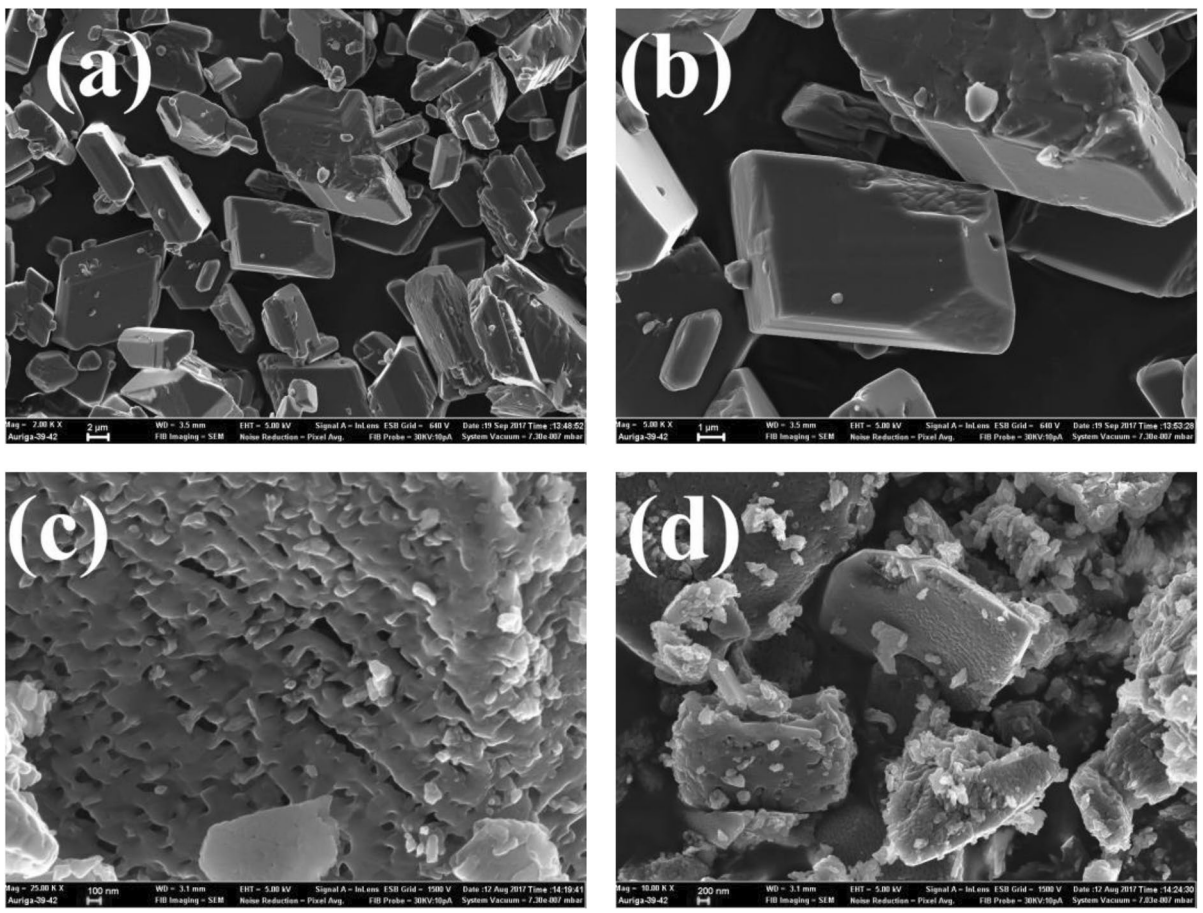

Fig. 3 SEM images showing the morphologies of the MOFs at various magnifications for **a** LaBDC (2 μm); **b** LaBDC (1 μm); **c** ZnBDC (100 nm); **d** ZnBDC (200 nm)

experimental time of adsorption of MB onto each adsorbent, and the adsorption trends are shown in Fig. 4a, b. The data showed that the rates of removal of MB in both adsorbents were fast, but equilibrium was reached quicker in the ZnBDC (at ≈ 30 min) compared to the LaBDC (at ≈ 120 min). The higher adsorption rate of the ZnBDC may not be unconnected to its larger pore size and volume, which makes it easier for the large MB molecules in solution to access the inner sections of the MOF structure, hence achieving equilibrium faster than the LaBDC with smaller pore size and volume. The adsorption trends observed in Fig. 4a, b (fast-steep section and a slow-plateau portion) have been attributed to the availability of vacant adsorption sites on the MOFs. The fast-steep section occurs are the beginning of the experiment when there are plenty of vacant adsorption sites and the rate of MB uptake is high. As equilibrium is approached, the rate reduces because vacant adsorption sites are fewer and the differences in uptake and desorption become increasingly insignificant until equilibrium, where it is equal with all adsorption sites filled, and the plateau appears in the rate curve (Diagboya et al., 2021a; Sera et al., 2022).

In order to explain the mechanism involved in the MB uptake on the MOFs, the experimental rate data were fitted to 4 nonlinear kinetics models: PFO, PSO, FPSOM, and the IPD. The kinetics parameters from the various model fittings are presented in Table 1. The table depicts that the PSO with the highest correlation coefficient ($r^2 = 0.910$) is the best fit for the adsorbent LaBDC and describes its MB adsorption

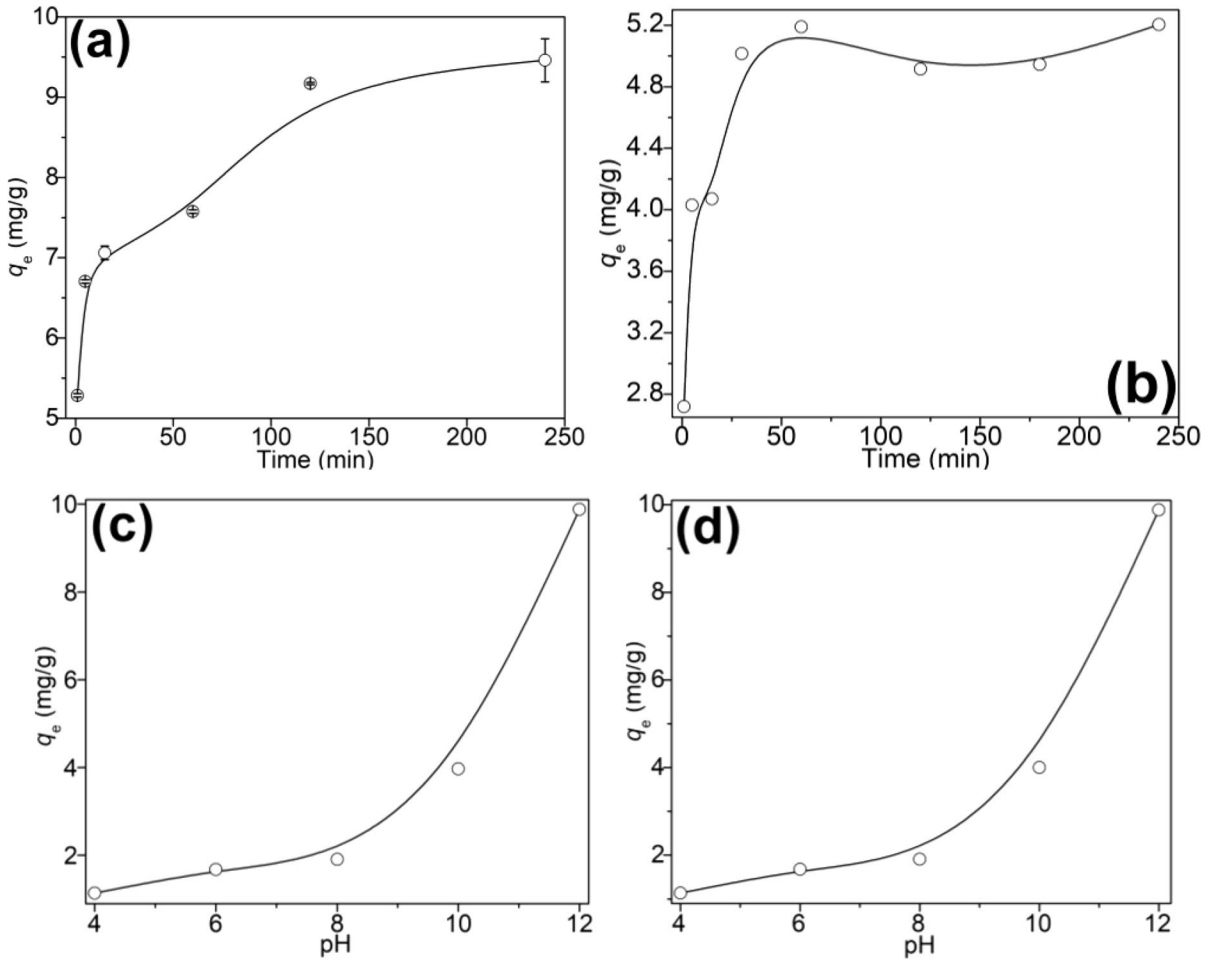

Fig. 4 Adsorption rates of MB at a varying time for **a** LaBDC and **b** ZnBDC adsorbents; adsorption trend at varying pH for **c** LaBDC and **d** ZnBDC

Table 1 Kinetic models parameter for MB adsorption onto the LaBDC and ZnBDC MOFs

Kinetic model	Parameter	LaBDC	ZnBDC
PFO	r^2	0.379	0.542
	q_e (mg/g)	8.0	2.4
	K	1.041	0.734
PSO	r^2	0.610	0.663
	q_e (mg/g)	8.4	2.5
	k	0.60	0.413
FPSO	r^2	0.910	0.606
	k_f	8.019	0.41
	q_e (mg/g)	84.6	2.6
	α	0.147	0.81
IPD	r^2	0.872	0.206
	k_{IPD}	0.267	0.051
	C (mg/g)	5.7	1.9
Experimental q_e	mg/g	9.1	2.5

data better than the other kinetic models, and the predicted q_e value correlates better with the experimental q_e values. This implied that the adsorption of MB from the aqueous solution onto LaBDC adsorbent was controlled mainly by electrostatic interactions (Diagboya et al., 2019). The rate constant (k_f) value indicated that the rate of MB uptake onto LaBDC was very fast. However, the experimental data fitting for the adsorbent ZnBDC (Table 1) showed an r^2 which correlates better with the PFO model. This model governed the rapid adsorption within the first few minutes of contact between the MB and ZnBDC when MB molecules outnumber available adsorption sites (Olu-Owolabi et al., 2022). Thus, for fast adsorption processes carried out over a wide time range but with equilibrium attained within the first few minutes of the experiment (as observed in Fig. 4b), the process is likely to obey the PFO.

Further analysis of the experimental data for the effect of time using the IPD model revealed the extent of parameter C, which defines the degree of surface uptake of the MB on both adsorbents (Zanele et al., 2021). The C values were 5.7 mg/g for LaBDC and 1.9 mg/g for ZnBDC; these implied that ≈ 63 and 76% of MB molecules, respectively, were involved in the surface adsorption phenomenon on both adsorbents (Diagboya et al., 2021b; Xikhongelo et al., 2021). The IPD plots (not shown) did not pass through the graph's origin, and this indicated intra-particle diffusion was not the rate-determining step, though it played a significant role in the adsorption process.

3.2.2 *Effect of pH on MB Adsorption on the MOFs*

The effect of pH on both MOFs was investigated at aqueous solution pH between 4 and 12. This was carried out because pH influences the behavior of both adsorbent and adsorbate during the adsorption process by affecting the charge density (and subsequently electrostatic interactions) surrounding either the adsorbate or adsorbent or both (Diagboya & Dikio, 2018a; Diagboya et al., 2019; Ebelegi et al., 2019; Nkutha et al., 2020). At lower pH regions, the MB removal was not favored on both adsorbents (Fig. 4a, d). However, as pH increased, the adsorption correspondingly increased until it reached the optimum pH of ≈ 12. This signifies that at low pH 4, the surfaces of the adsorbents were heavily protonated (H^+), masking the negatively charged surfaces generated by the carboxylic groups in the MOFs. This consequently led to the creation of electrostatic repulsive forces between the positively charged adsorbate (MB) molecules and the protonated (positive) adsorption sites. As the pH increased toward the pHpzc (6.8: for LaBDC and ZnBDC), the concentration of the H^+ decreased resulting in a gradual buildup of negative charges on the surface of both adsorbents, leading to the increased electrostatic attraction between the adsorbents and the cationic molecules of the adsorbate (Diagboya et al., 2019; Fallah Shojaei et al., 2018; Khodaie et al., 2013; Konicki & Pełech, 2019). This is the adduced reason for the gradual increase in the adsorption of the cationic MB dye molecules until optimum uptake of MB was attained by the two adsorbents at pH 12.

3.2.3 *Equilibrium MB Adsorption and Dynamics of the Process*

The understanding of the dynamics of the adsorption of MB on both adsorbents was gained via equilibrium experiments by varying the concentration of the adsorbate (MB) solution from 20 to 60 mg/L and the ambient temperature from 300 to 320 K (Zanele et al., 2021). The trends observed are presented in Fig. 5a–c. The trend observed for both LaBDC and ZnBDC exhibited an increase in the adsorption of

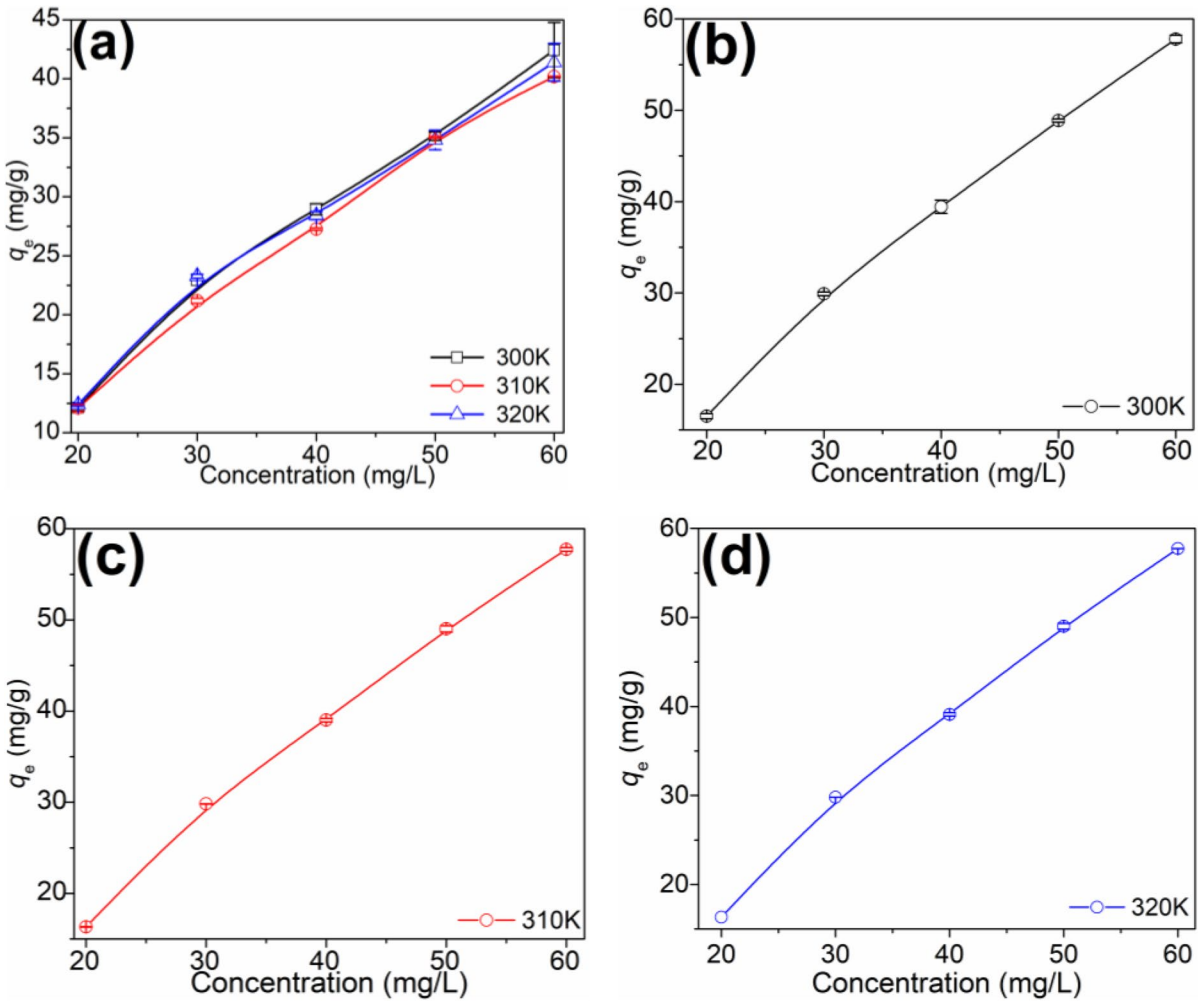

Fig. 5 Plot of effect of concentration and temperature on adsorption of MB onto **a** LaBDC; effect of concentration on MB adsorption at varying temperature onto ZnBDC at **b** 300 K, **c** 310 K, and **d** 320 K

MB as the concentration of MB was increased at all temperatures. This linear increase may be an indication that the adsorbents had available surface sites to accommodate the MB molecules arising from increased concentration or that multi-layer adsorption was involved in the increasing uptake; the latter was tested using the Freundlich adsorption isotherm model. However, comparing the adsorption of MB as concentration increased over varying temperatures showed that there were no significant differences in the MB adsorption when the temperature varied from 300 to 320 K. The overall trend tended towards an exothermic process. This trend could have arisen due to weakened adsorptive forces between the active sites of the MOFs and MB species vicinal molecules of the adsorbed phase when the temperatures were increased (Olu-Owolabi et al., 2012). Another reason could be due to an increase in kinetic energy, which enhanced MB solubility and made the MB molecules move faster and away from the adsorbent surfaces, thus leading to the desorption of the adsorbed MB molecules (Al-Degs et al., 2008; Olu-Owolabi et al., 2012, 2016).

The equilibrium data at 300, 310, and 320 K for the two adsorbents were further evaluated using the Langmuir and Freundlich isotherm models to a gain better understanding of the adsorption process. The values of the parameters generated from Origin Pro

Table 2 Isotherm parameters for MB adsorption on LaBDC and ZnBDC at 300, 310, and 320 K

Isotherm	Parameter	LaBDC			ZnBDC		
		300 K	310 K	320 K	300 K	310 K	320 K
Langmuir	Q_o (mg/g)	7844.6	8772.2	692.0	17,159.3	21,023.2	20,845.0
	r^2	0.982	0.988	0.979	0.987	0.987	0.987
	b	9.092	7.796	0.000	5.660	4.607	4.646
Freundlich	K_f (L/g)	0.67	0.60	0.70	0.828	0.796	0.800
	r^2	0.981	0.981	0.980	0.987	0.989	0.989
	n	1.01	1.00	0.90	1.041	1.049	1.049
Q_o (mg/g) Experimental q_e		40.00	38.00	35.00	55.0	55.0	55.0

2015 software are shown in Table 2. The comparative evaluation of the values of the Langmuir and Freundlich adsorption isotherm parameters for LaBDC and ZnBDC showed that the r^2 of both models at the different temperatures were significantly close to unity, implying that both isotherm models could be reasonably used to describe the process. The Langmuir adsorption isotherm model proposes monolayer adsorption on homogeneous surface adsorption sites with similar energy, while the Freundlich adsorption isotherm model suggests a multi-layer adsorption process (Diagboya et al., 2014). The good fit of these data to the Langmuir model suggests that the MB molecules were adsorbed on similar adsorption sites with almost equal adsorption energy. However, the good fit to the Freundlich model indicated that there was multilayer adsorption due to π–π interactions between the aromatic rings of MB initially adsorbed on the MOFs' surface and aromatic rings of MB molecules from the solution (Diagboya et al., 2014). It has been reported that when adsorption occurs, whether by electrostatic interaction (on similar or dissimilar sites) or via multilayer adsorption, but with forces of interaction of similar energy, the data tends to fit both models (Diagboya et al., 2016; Weber et al., 1992).

The thermodynamics parameters (ΔH^o, ΔS^o, and ΔG^o) were generated with the experimental data at the three different temperatures for each of the adsorbents (Table 3). Table 3 reveals negative ΔG^o values for the adsorption of MB by these adsorbents, indicating a spontaneous and feasible process. The low values of ΔS^o for these adsorbents were suggestive of slightly increased randomness at the solid–liquid interface during the adsorption process. As suggested above, the negative ΔH^o of ZnBDC is indicative of an exothermic process, while the value for the LaBDC suggests that a further increase in temperature may enhance the adsorption process. The values of the ΔH^o parameter for both MOFs were below the 40 kJ/mol value for physisorption processes, and this implied that the adsorption process was physisorption in nature (Akpotu et al., 2022a).

Table 3 Thermodynamic parameters for the adsorption of MB on LaBDC and ZnBDC

Adsorbent	ΔH^o (kJ/mol)	ΔS^o (Jmol/K)	ΔG^o (kJ/mol)		
			300 K	310 K	320 K
LaBDC	6.24	0.03	−2.36	−2.23	−2.94
ZnBDC	−15.34	−0.01	−8.02	−7.31	−7.55

Table 4 Comparison of MB adsorption by reported MOF-based adsorbents

Adsorbent	q_e (mg/g)	Reference
MOF-235	187	(Haque et al., 2011)
Fe-MOF-5	161.3	(Fallah Shojaei et al., 2018)
$Fe_3O_4/Cu_3(BTC)_2$	84	(Zhao et al., 2015)
MIL-101(Fe)	58.8	(Eltaweil et al., 2020)
ZnBDC	55.0	This study
$H_6P_2W_{18}O_{62}$/MOF-5	51.81	(Liu et al., 2016)
MIL-53	45.21	(Li et al., 2015)
Cu-BTC	45.05	(Li et al., 2021)
UiO-66-NO_2	41.70	(Dinh et al., 2021)
LaBDC	35.00	This study
MOF-5	35.00	(Gong et al., 2018)

The obtained MOF adsorption capacities of both adsorbents for MB were compared with the results of MOFs reported in the literature (Table 4). This

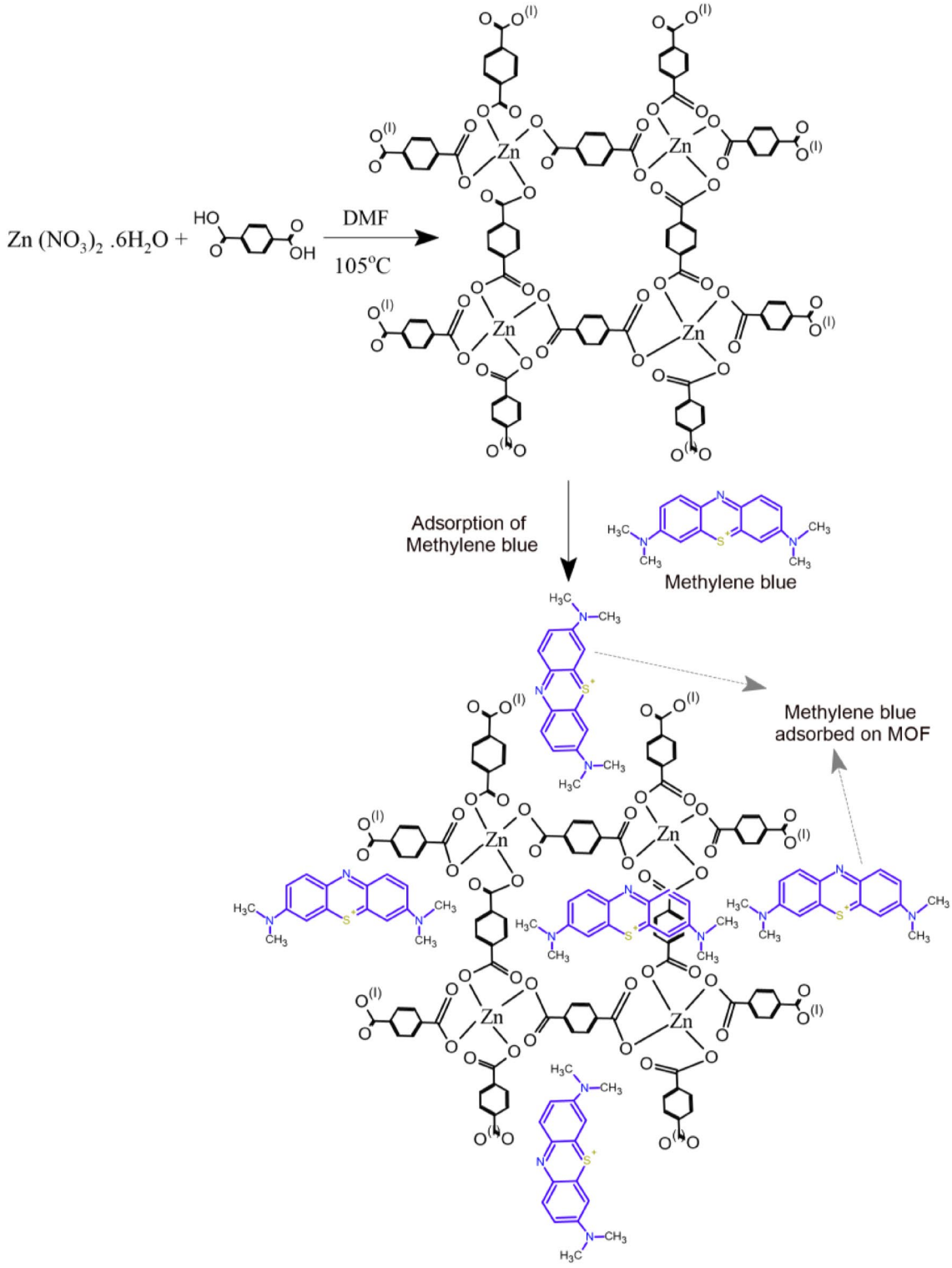

Fig. 6 Scheme for the synthesis of MOF and adsorption of MB

comparison indicated that though both MOFs were similar in structure, the adsorption capacity of MOFs depends on the coordinating metal ion; thus, Zn-MOF exhibited better adsorption capacity than the LaBDC MOF. These MOFs were also better than several MOFs reported in the literature. A brief scheme showing the synthesis and adsorption of the MB on the MOF is shown in Fig. 6.

4 Conclusions

The MOF adsorbents, lanthanum-1, 4-benzene dicarboxylate (LaBDC) and zinc-1, 4-benzene dicarboxylate (ZnBDC), were successfully prepared via the reflux-controlled solvothermal process and used for the adsorption of the cationic dye methylene blue (MB). The MOFs were well characterized using XRD, SEM/EDX, FTIR, and BET, and these showed that the MOFs were crystalline with a cubic structure for LaBDC and an interwoven structure for ZnBDC. The metal–oxygen (M–O) linkage was expressed by both MOFs, which were porous, with thermal stability which was above 450 °C. The adsorption kinetics followed the FPSOM, Langmuir, and Freundlich models, which signified the occurrence of a complex adsorption phenomenon. The pH of optimum adsorption was recorded at pH 12, and the maximum adsorption values of MB for LaBDC and ZnBDC are 35.0 and 55.0 mg/g, respectively. The adsorption process was physisorption in nature, spontaneous and exothermic. Thus, these MOFs have the potential for MB sequestration from water, but further modification and enhancements of the surface functional groups will be necessary to achieve far better performance.

Acknowledgements We acknowledge the support of the Faculty of Applied and Computer Science and the Research Directorate of Vaal University of Technology, Vanderbijlpark, South Africa.

Author Contribution Emmanuel B. AttahDaniel: Study conception, design, data collection, and draft writing, reviewing, and editing. Paul N. Diagboya: Study conception, design, data collection, draft writing, reviewing, and editing, supervising, and funding. Fanyana M. Mtunzi: Study conception, design, supervising, and funding. Donbebe Wankasi: Study conception, design, supervising, and funding. Nimibofa Ayawei: Study conception, design, supervising, and funding. Ezekiel D. Dikio: Study conception, design, data collection, supervising, reviewing, and funding.

Data Availability The datasets used and analyzed during the current study are available from the corresponding author upon reasonable request.

Materials Availability The datasets used and analyzed during the current study are available from the corresponding author upon reasonable request.

Declarations

Competing Interests The authors declare no competing interests.

References

Aghajanloo, M., Rashidi, A. M., & Moosavian, M. A. (2014). Synthesis of zinc-organic frameworks nano adsorbent and their application for methane adsorption. *Journal of Chemical Engineering & Process Technology, 5*, 1.

Akpotu, S. O., Lawal, I. A., Diagboya, P. N., Mtunzi, F. M., & Ofomaja, A. E. (2022b). Engineered geomedia kaolin clay-reduced graphene oxide–polymer composite for the remediation of olaquindox from water. *ACS Omega, 7*, 34054–34065.

Akpotu, S. O., Diagboya, P. N., Lawal, I. A., Sanni, S. O., Pholosi, A., Mtunzi, F. M., Ofomaja, A. E. (2022a) Designer composite of montmorillonite-reduced graphene oxide-PEG polymer for water treatment: Enrofloxacin sequestration and cost analysis. *Chemical Engineering Journal*, 139771 https://doi.org/10.1016/j.cej.2022a.139771

Al-Degs, Y. S., El-Barghouthi, M. I., El-Sheikh, A. H., & Walker, G. M. (2008). Effect of solution pH, ionic strength, and temperature on adsorption behavior of reactive dyes on activated carbon. *Dyes and Pigments, 77*, 16–23.

Ali, I. (2012). New generation adsorbents for water treatment. *Chemical Reviews, 112*, 5073–5091.

Altenor, S., Carene, B., Emmanuel, E., Lambert, J., Ehrhardt, J.-J., & Gaspard, S. (2009). Adsorption studies of methylene blue and phenol onto vetiver roots activated carbon prepared by chemical activation. *Journal of Hazardous Materials, 165*, 1029–1039.

Ayati, A., Shahrak, M. N., Tanhaei, B., & Sillanpää, M. (2016). Emerging adsorptive removal of azo dye by metal–organic frameworks. *Chemosphere, 160*, 30–44.

Aygün, A., Yenisoy-Karakaş, S., & Duman, I. (2003). Production of granular activated carbon from fruit stones and nutshells and evaluation of their physical, chemical and adsorption properties. *Microporous and Mesoporous Materials, 66*, 189–195.

Bosch, M., Yuan, S., Rutledge, W., & Zhou, H.-C. (2017). Stepwise synthesis of metal–organic frameworks. *Accounts of Chemical Research, 50*, 857–865.

Chen, M., Huo, C., Li, Y., & Wang, J. (2016). Selective adsorption and efficient removal of phosphate from aqueous medium with graphene–lanthanum composite. *ACS Sustainable Chemistry & Engineering, 4*, 1296–1302.

Chen, W., Yang, J., Zhao, Y., Hu, Y., & Xiang, B. (2017). Synthesis and luminescence properties of brick-shaped lanthanum–organic frameworks with mesoporous and macroporous architectures. *Luminescence, 32*, 1289–1293.

DeCoste, J. B., & Peterson, G. W. (2014). Metal–organic frameworks for air purification of toxic chemicals. *Chemical Reviews, 114*, 5695–5727.

Diagboya, P. N., & Dikio, E. D. (2018a). Dynamics of mercury solid phase extraction using Barbula lambarenensis. *Environmental Technology & Innovation, 9*, 275–284.

Diagboya, P. N., & Dikio, E. D. (2018b). Scavenging of aqueous toxic organic and inorganic cations using novel facile magneto-carbon black-clay composite adsorbent. *Journal of Cleaner Production, 180*, 71–80.

Diagboya, P. N., Olu-Owolabi, B. I., Zhou, D., & Han, B.-H. (2014). Graphene oxide–tripolyphosphate hybrid used as a potent sorbent for cationic dyes. *Carbon, 79*, 174–182.

Diagboya, P. N., Olu-Owolabi, B. I., & Adebowale, K. O. (2016). Distribution and interactions of pentachlorophenol in soils: The roles of soil iron oxides and organic matter. *Journal of Contaminant Hydrology, 191*, 99–106.

Diagboya, P. N., Mmako, H. K., Dikio, E. D., & Mtunzi, F. M. (2019). Synthesis of amine and thiol dual functionalized graphene oxide for aqueous sequestration of lead. *Journal of Environmental Chemical Engineering, 7*, 103461.

Diagboya, P. N., Mtunzi, F. N., Adebowale, K. O., & Olu-Owolabi, B. I. (2021b). Assessment of the effects of soil organic matter and iron oxides on the individual sorption of two polycyclic aromatic hydrocarbons. *Environmental Earth Sciences, 80*, 227.

Diagboya, P. N., Mtunzi, F. M., Adebowale, K. O., Düring, R.-A., Olu-Owolabi, B. I. (2021a) Comparative empirical evaluation of the aqueous adsorptive sequestration potential of low-cost feldspar-biochar composites for ivermectin. *Colloids and Surfaces A: Physicochemical and Engineering Aspects*, 127930.

Dikio, E. D., & Farah, A. M. (2013). Synthesis, characterization and comparative study of copper and zinc metal organic frameworks. *Chemical Science Transactions, 2*, 1386–1394.

Dinh, H. T., Tran, N. T., Trinh, D. X. (2021) Investigation into the adsorption of methylene blue and methyl orange by UiO-66-NO2 nanoparticles. *Journal of Analytical Methods in Chemistry*, 2021.

Ebelegi, A. N., Ayawei, N., Wankasi, D., Dikio, E. D., Diagboya, P. N., & Mtunzi, F. M. (2019). Covalently bonded polyamidoamine functionalized silica used as a Pb(II) scavenger from aqueous solution. *Journal of Environmental Chemical Engineering, 7*, 103214.

Eltaweil, A. S., Abd El-Monaem, E. M., Omer, A. M., Khalifa, R. E., Abd El-Latif, M. M., & El-Subruiti, G. M. (2020). Efficient removal of toxic methylene blue (MB) dye from aqueous solution using a metal-organic framework (MOF) MIL-101 (Fe): Isotherms, kinetics, and thermodynamic studies. *Desalination and Water Treatment, 189*, 395–407.

FallahShojaei, A., Tabatabaeian, K., & Zebardast, M. (2018). Ferric ion modified nano-MOF-5 synthesized by direct mixing approach: A highly efficient adsorbent for methylene blue dye. *Scientia Iranica, 25*, 1323–1334.

Farooq Khan, M., Ahmed, H., AbdulkareemAlmashhadani, H., Al-Bahrani, M., Ullah Khan, A., Ali, S., Gul, N., Hassan, T., Ismail, A., & Zahid, M. (2022a). Sustainable adsorptive removal of high concentration organic contaminants from water using biodegradable gum-acacia integrated magnetite nanoparticles hydrogel adsorbent. *Inorganic Chemistry Communications, 145*, 110057.

Farooq Khan, M., Jamal, A., Jacquline Rosy, P., Alguno, A. C., Ismail, M., Khan, I., Ismail, A., & Zahid, M. (2022b). Eco-friendly elimination of organic pollutants from water using graphene oxide assimilated magnetic nanoparticles adsorbent. *Inorganic Chemistry Communications, 139*, 109422.

Freundlich, H. (1907). Über die adsorption in lösungen. *Zeitschrift Für Physikalische Chemie, 57*, 385–470.

Gangadhar, G., Maheshwari, U., & Gupta, S. (2012). Application of nanomaterials for the removal of pollutants from effluent streams. *Nanoscience & Nanotechnology-Asia, 2*, 140–150.

Ge, J. C., Yoon, S. K., & Choi, N. J. (2018). Application of fly ash as an adsorbent for removal of air and water pollutants. *Applied Sciences, 8*, 1116.

Gong, W., Du, X., Liu, X., Ke, X., Yang, S. (2018) Achieving adsorption of cationic dyes by the composites based on H3PMo12O40 decorating metal organic frameworks.

Guo, J.-Z., Li, B., Liu, L., & Lv, K. (2014). Removal of methylene blue from aqueous solutions by chemically modified bamboo. *Chemosphere, 111*, 225–231.

Haerifar, M., & Azizian, S. (2014). Fractal-like kinetics for adsorption on heterogeneous solid surfaces. *The Journal of Physical Chemistry C, 118*, 1129–1134.

Hameed, B., & Hakimi, H. (2008). Utilization of durian (Durio zibethinus Murray) peel as low cost sorbent for the removal of acid dye from aqueous solutions. *Biochemical Engineering Journal, 39*, 338–343.

Haque, E., Jun, J. W., & Jhung, S. H. (2011). Adsorptive removal of methyl orange and methylene blue from aqueous solution with a metal-organic framework material, iron terephthalate (MOF-235). *Journal of Hazardous Materials, 185*, 507–511.

Hasan, Z., & Jhung, S. H. (2015). Removal of hazardous organics from water using metal-organic frameworks (MOFs): Plausible mechanisms for selective adsorptions. *Journal of Hazardous Materials, 283*, 329–339.

Hasan, Z., Choi, E.-J., & Jhung, S. H. (2013). Adsorption of naproxen and clofibric acid over a metal–organic framework MIL-101 functionalized with acidic and basic groups. *Chemical Engineering Journal, 219*, 537–544.

Horcajada, P., Serre, C., Vallet-Regí, M., Sebban, M., Taulelle, F., & Férey, G. (2006). Metal–organic frameworks as efficient materials for drug delivery. *Angewandte Chemie, 118*, 6120–6124.

Hosseini, S. A., Mashaykhi, S., & Babae, S. (2016). Graphene oxide/zinc oxide nanocomposite: A superior adsorbent for removal of methylene blue statistical analysis by response surface methodology (RSM). *South African Journal of Chemistry, 69*, 105–112.

Hosseini, S., Paymanfar, R., Afshari, T., & Hosseini, S. (2020). Preparation of MWCNT/Ba0. 2Sr0. 2La0. 6MnO3/PANI nanocomposites and investigation of its electromagnetic properties in KU-band. *International Journal of Physical Sciences, 15*, 171–181.

Jahagirdar, S. S., Shrihari, S., & Manu, B. (2015). Reuse of incinerated textile mill sludge as adsorbent for dye removal. *KSCE Journal of Civil Engineering, 19*, 1982–1986.

Juang, R.-S., Wu, F.-C., & Tseng, R.-L. (2002). Characterization and use of activated carbons prepared from bagasses for liquid-phase adsorption. *Colloids and Surfaces a: Physicochemical and Engineering Aspects, 201*, 191–199.

Kadirvelu, K., Palanival, M., Kalpana, R., & Rajeswari, S. (2000). Activated carbon from an agricultural by-product, for the treatment of dyeing industry wastewater. *Bioresource Technology, 74*, 263–265.

Khodaie, M., Ghasemi, N., Moradi, B., Rahimi, M. (2013) Removal of methylene blue from wastewater by adsorption onto ZnCl2 activated corn husk carbon equilibrium studies. *Journal of Chemistry*, 2013.

Konicki, W., Pełech, I. (2019) Removing cationic dye from aqueous solutions using as-grown and modified multi-walled carbon nanotubes. *Polish Journal of Environmental Studies*, 28.

Lagergren, S. K. (1898). About the theory of so-called adsorption of soluble substances. *Sven. Vetenskapsakad. Handingarl, 24*, 1–39.

Langmuir, I. (1916). The constitution and fundamental properties of solids and liquids. Part I. Solids. *Journal of the American Chemical Society, 38*, 2221–2295.

Li, H., Eddaoudi, M., Groy, T. L., & Yaghi, O. (1998). Establishing microporosity in open metal− organic frameworks: Gas sorption isotherms for Zn (BDC)(BDC= 1, 4-benzenedicarboxylate). *Journal of the American Chemical Society, 120*, 8571–8572.

Li, C., Xiong, Z., Zhang, J., & Wu, C. (2015). The strengthening role of the amino group in metal–organic framework MIL-53 (Al) for methylene blue and malachite green dye adsorption. *Journal of Chemical & Engineering Data, 60*, 3414–3422.

Li, Y., Gao, C., Jiao, J., Cui, J., Li, Z., & Song, Q. (2021). Selective adsorption of metal–organic framework toward methylene blue: Behavior and mechanism. *ACS Omega, 6*, 33961–33968.

Lin, Y. S. (2015). Metal organic framework membranes for separation applications. *Current Opinion in Chemical Engineering, 8*, 21–28.

Lin, S., Song, Z., Che, G., Ren, A., Li, P., Liu, C., & Zhang, J. (2014). Adsorption behavior of metal–organic frameworks for methylene blue from aqueous solution. *Microporous and Mesoporous Materials, 193*, 27–34.

Lin, J. M., He, C. T., Liu, Y., Liao, P. Q., Zhou, D. D., Zhang, J. P., & Chen, X. M. (2016). A metal–organic framework with a pore size/shape suitable for strong binding and close packing of methane. *Angewandte Chemie, 128*, 4752–4756.

Liu, B., Shioyama, H., Akita, T., & Xu, Q. (2008). Metal-organic framework as a template for porous carbon synthesis. *Journal of the American Chemical Society, 130*, 5390–5391.

Liu, Y., Ng, Z., Khan, E. A., Jeong, H.-K., Ching, C.-B., & Lai, Z. (2009). Synthesis of continuous MOF-5 membranes on porous α-alumina substrates. *Microporous and Mesoporous Materials, 118*, 296–301.

Liu, X., Gong, W., Luo, J., Zou, C., Yang, Y., & Yang, S. (2016). Selective adsorption of cationic dyes from aqueous solution by polyoxometalate-based metal–organic framework composite. *Applied Surface Science, 362*, 517–524.

Malekbala, M. R., Hosseini, S., Yazdi, S. K., Soltani, S. M., & Malekbala, M. R. (2012). The study of the potential capability of sugar beet pulp on the removal efficiency of two cationic dyes. *Chemical Engineering Research and Design, 90*, 704–712.

Malik, P. K. (2003). Use of activated carbons prepared from sawdust and rice-husk for adsorption of acid dyes: A case study of Acid Yellow 36. *Dyes and Pigments, 56*, 239–249.

Mohamed, M. M. (2004). Acid dye removal: Comparison of surfactant-modified mesoporous FSM-16 with activated carbon derived from rice husk. *Journal of Colloid and Interface Science, 272*, 28–34.

Mohammed, E., Jaarrod, F. E. (2010) Insight into the development of metal-organic materials (MOMs). *At Zeolite-like Metal-Organic Frameworks (ZMOFs)." 32 - 33.*, 32 - 33.

Mulfort, K. L., Farha, O. K., Stern, C. L., Sarjeant, A. A., & Hupp, J. T. (2009). Post-synthesis alkoxide formation within metal− organic framework materials: A strategy for incorporating highly coordinatively unsaturated metal ions. *Journal of the American Chemical Society, 131*, 3866–3868.

Mulugeta, M., & Lelisa, B. (2014). Removal of methylene blue (Mb) dye from aqueous solution by bioadsorption onto untreated Parthenium hystrophorous weed. *Mod. Chem. Appl, 2*, 146.

Munoz, B., Ramila, A., Perez-Pariente, J., Diaz, I., & Vallet-Regi, M. (2003). MCM-41 organic modification as drug delivery rate regulator. *Chemistry of Materials, 15*, 500–503.

Nakhla, J. (2009). Metal organic frameworks (MOFs). *Aldrich ChemFiles, 9*, 19.

Namasivayam, C., & Kavitha, D. (2002). Removal of Congo red from water by adsorption onto activated carbon prepared from coir pith, an agricultural solid waste. *Dyes and Pigments, 54*, 47–58.

Nkutha, C. S., Diagboya, P. N., Mtunzi, F. M., & Dikio, E. D. (2020). Application of eco-friendly multifunctional porous graphene oxide for adsorptive sequestration of chromium in aqueous solution. *Water Environment Research, 92*, 1070–1079.

Okoli, C. P., Diagboya, P. N., Anigbogu, I. O., Olu-Owolabi, B. I., & Adebowale, K. O. (2017). Competitive biosorption of Pb (II) and Cd (II) ions from aqueous solutions using chemically modified moss biomass (Barbula lambarenensis). *Environmental Earth Sciences, 76*, 1–10.

Olu-Owolabi, B. I., Diagboya, P. N., & Ebaddan, W. C. (2012). Mechanism of Pb2+ removal from aqueous solution using a nonliving moss biomass. *Chemical Engineering Journal, 195–196*, 270–275.

Olu-Owolabi, B. I., Diagboya, P. N., Mtunzi, F. M., & Düring, R.-A. (2021). Utilizing eco-friendly kaolinite-biochar composite adsorbent for removal of ivermectin in aqueous media. *Journal of Environmental Management, 279C*, 111619.

Olu-Owolabi, B. I., Diagboya, P. N., Mtunzi, F. M., Adebowale, K. O., & Düring, R.-A. (2022). Empirical aspects of an emerging agricultural pesticide contaminant retention on two sub-Saharan soils. *Gondwana Research, 105*, 311–319.

Olu-Owolabi, B. I., Diagboya, P. N., Okoli, C. P., Adebowale, K. O. (2016) Sorption behaviour of pentachlorophenol in sub-Saharan tropical soils: Soil types sorption dynamics. *Environmental Earth Sciences*, 75.

Prabhu, S. M., Imamura, S., & Sasaki, K. (2019). Mono-, di-, and tricarboxylic acid facilitated lanthanum-based organic frameworks: Insights into the structural stability and mechanistic approach for superior adsorption of arsenate from water. *ACS Sustainable Chemistry & Engineering, 7*, 6917–6928.

Savin, I.-I.; Butnaru, R. (2008) Wastewater characteristics in textile finishing mills. *Environmental Engineering & Management Journal (EEMJ)*, 7.

Schoedel, A., Ji, Z., & Yaghi, O. M. (2016). The role of metal–organic frameworks in a carbon-neutral energy cycle. *Nature Energy, 1*, 1–13.

Sera, P. R., Diagboya, P. N., Akpotu, S. O., Mtunzi, F. M., & Chokwe, T. B. (2022). Potential of valourized Moringa oleifera seed waste modified with activated carbon for toxic metals decontamination in conventional water treatment. *Bioresource Technology Reports, 16*, 100881.

Shooto, N. D., & Dikio, E. D. (2018). Highly porous MOF adsorbent for wastewater treatment. *Asian Journal of Chemistry, 30*, 1723–1730.

Shooto, N., Ayawei, N., Wankasi, D., Sikhwivhilu, L., & Dikio, E. (2016). Study on cobalt metal organic framework material as adsorbent for lead ions removal in aqueous solution. *Asian Journal of Chemistry, 28*, 277.

Sriram, G., Bendre, A., Mariappan, E., Altalhi, T., Kigga, M., Ching, Y. C., Jung, H.-Y., Bhaduri, B., Kurkuri, M. (2021) Recent trends in the application of metal-organic frameworks (MOFs) for the removal of toxic dyes and their removal mechanism-A review. *Sustainable Materials and Technologies*, e00378.

Starukh, G. (2017). Photocatalytically enhanced cationic dye removal with Zn-Al layered double hydroxides. *Nanoscale Research Letters, 12*, 1–8.

Valix, M., Cheung, W., & McKay, G. (2004). Preparation of activated carbon using low temperature carbonisation and physical activation of high ash raw bagasse for acid dye adsorption. *Chemosphere, 56*, 493–501.

Wang, L., Wu, Y., Chen, F., & Yang, X. (2014). Photocatalytic enhancement of Mg-doped ZnO nanocrystals hybridized with reduced graphene oxide sheets. *Progress in Natural Science: Materials International, 24*, 6–12.

Wang, H., Jia, S., Wang, H., Li, B., Liu, W., Li, N., Qiao, J., & Li, C.-Z. (2017). A novel-green adsorbent based on betaine-modified magnetic nanoparticles for removal of methyl blue. *Science Bulletin, 62*, 319–325.

Wang, L., Hu, G., Lyu, F., Yue, T., Tang, H., Han, H., Yang, Y., Liu, R., & Sun, W. (2019). Application of red mud in wastewater treatment. *Minerals, 9*, 281.

Weber, W. J., Jr., & Morris, J. C. (1963). Kinetics of adsorption on carbon from solution. *Journal of the Sanitary Engineering Division, 89*, 31–59.

Weber, W. J., Jr., McGinley, P. M., & Katz, L. E. (1992). A distributed reactivity model for sorption by soils and sediments. 1. Conceptual basis and equilibrium assessments. *Environmental Science & Technology, 26*, 1955–1962.

Wlodarski, M., Matti, P., & Malgorzata, N. (2020). Infrared absorption study of Zn–S hybrid and ZnS ultrathin films deposited on porous AAO ceramic support. *Coatings, 10*, 459.

Xikhongelo, R. V., Mtunzi, F. M., Diagboya, P. N., Olu-Owolabi, B. I., & Düring, R.-A. (2021). Polyamidoamine-functionalized graphene oxide–SBA-15 mesoporous composite: Adsorbent for aqueous arsenite, cadmium, ciprofloxacin, ivermectin, and tetracycline. *Industrial & Engineering Chemistry Research, 60*, 3957–3968.

Zanele, Z. P., Mtunzi, F. M., Nelana, S. M., Ebelegi, A. N., Ayawei, N., Dikio, E. D., Wankasi, D., & Diagboya, P. N. (2021). Metals and Antibiotics as aqueous sequestration targets for magnetic polyamidoamine-grafted SBA-15. *Langmuir, 37*, 9764–9773.

Zhang, C., Li, P., Huang, W., & Cao, B. (2016). Selective adsorption and separation of organic dyes in aqueous solutions by hydrolyzed PIM-1 microfibers. *Chemical Engineering Research and Design, 109*, 76–85.

Zhang, K.-D., Tsai, F.-C., Ma, N., Xia, Y., Liu, H.-L., Zhan, X.-Q., Yu, X.-Y., Zeng, X.-Z., Jiang, T., & Shi, D. (2017). Adsorption behavior of high stable Zr-based MOFs for the removal of acid organic dye from water. *Materials, 10*, 205.

Zhao, X., Liu, S., Tang, Z., Niu, H., Cai, Y., Meng, W., Wu, F., & Giesy, J. P. (2015). Synthesis of magnetic metal-organic framework (MOF) for efficient removal of organic dyes from water. *Scientific Reports, 5*, 1–10.

Zhu, B.-J., Yu, X.-Y., Jia, Y., Peng, F.-M., Sun, B., Zhang, M.-Y., Luo, T., Liu, J.-H., & Huang, X.-J. (2012). Iron and 1, 3, 5-benzenetricarboxylic metal–organic coordination polymers prepared by solvothermal method and their application in efficient As (V) removal from aqueous solutions. *The Journal of Physical Chemistry C, 116*, 8601–8607.